

Ab initio modelling of defect properties with substitutional and interstitials elements in steels and Zr alloys

Christophe Domain *

*Electricité de France, EDF – R&D, Dpt Matériaux et Mécanique des Composants, Les Renardières, F-77250 Moret sur Loing, France
Laboratoire de Métallurgie Physique et Génie des Matériaux, UMR 8517, Bât. C6, Université Lille I,
F-59655 Villeneuve d'Ascq cédex, France*

Abstract

In alloys, the different elements interact with each other as well as with the various defects present: point defects or extended defects (stacking faults, dislocations, grain boundaries). These interactions are responsible for the elementary mechanisms governing the kinetics of the system, and they are among the key parameters to model the time evolution of the microstructure, under ageing or irradiation. Indeed the microstructure properties are directly linked to the chemical interactions between the different constituting elements, and these defects. Ab initio methods allow to determine properties such as defect formation, binding or migration energies. These crucial quantities can shed light on the various mechanisms involved in the evolution of the microstructure as well as be used as input for various models. In this article, data obtained by ab initio calculation of point defects (vacancies and self-interstitial atoms, foreign interstitial defects (C, N, H and He) in different matrix element (Fe and Zr) as well as of some substitutional elements (Cu, Ni, Mn, Si, Cr and P...)) in bcc Fe will be presented and discussed. When available, comparison with experimental data will be made in order to assess the validity of the results. The link between the obtained atomic quantities and the related consequences on the macroscopic properties will be discussed.

© 2006 Elsevier B.V. All rights reserved.

PACS: 61.72.–y; 71.15.Mb; 71.20.Be; 61.82.Bg

1. Introduction

In the field of nuclear energy, the increase of the lifetime and the improvement of the safety of the installations are a technological and economical

issue, in which the evolution of the properties of structural materials is one of the key parameter. The same questions have to be addressed also about the materials that will be used in the next generation of fission as well as fusion reactors.

The evolution of the materials properties under severe conditions, such as radiation damage, is a multiscale phenomenon, starting at the interaction of the energetic particle with matter (at the picosecond and nanometre scales) which produces point

* Address: Electricité de France, EDF – R&D, Dpt Matériaux et Mécanique des Composants, Les Renardières, F-77250 Moret sur Loing, France. Tel.: +33 1 60 73 60 44; fax: +33 1 60 73 68 89.
E-mail address: christophe.domain@edf.fr

defects and displacement cascades and leading up to the component evolution (at the year/decade and macroscopic scales) with formation of large defects or solute clusters and changes of the mechanical properties. The understanding and the prediction of the properties of the material evolution require knowledge at the different scales involved to somehow form a complete picture of what is happening. From the modelling point of view, it implies the linking and/or coupling of different codes based on different techniques (ab initio, classical molecular dynamics, kinetic Monte Carlo, mean field, dislocation dynamics, finite elements).

In order to develop predictive tools, all the mechanisms intervening have to be included. The materials used contain solute species in more or less dilute proportions, around 1% in pressure vessel steels and in cladding materials (Zr alloys), around 10% for FeCr alloys and in larger proportion for austenitic steels. The presence of interstitial elements such as C, N or H also have important consequences on the material properties even if their amount is low.

Multiscale modelling of materials is in progress [1–3] and will contribute to the development of such tools. A first tool devoted to radiation damage in pressure vessel, ‘virtual test reactor’ has been developed within an international collaboration, called REVE [4,5]. The construction of such tools gathered on a same platform is under development within the PERFECT European project devoted to pressure vessel as well austenitic steels, including physics and microstructure, mechanical as well as corrosion modelling [6].

Some of the most important elementary mechanisms involved in the modelling of the microstructure under irradiation are (i) the interactions among defects (point defects and extended ones such as dislocation or grain boundary) and between defect and chemical elements present in the matrix; (ii) the diffusion properties of point defects; (iii) the dynamical features of these interactions. The irradiation effects result from a synergy between the defects produced and the chemistry of the matrix. For instance, elastic interactions alone cannot explain the behaviour of two interacting foreign interstitial atoms [7], and in general, the classical elastic theory does not apply at the atomic scale or when chemical interactions are stronger than elastic or volume effects.

Ab initio calculation is nowadays the state of the art method to obtain insight and data on the elementary atomic mechanisms. These calculations

have involved most of the time ordered structures and phase stability, and in a less extent the effect of the presence of defects, from point defects up to linear defects or planar defects. In order to simulate representative systems, the treatment of system containing a few hundreds of atoms is/would be required. Thus, the resolution and implementation of the quantum mechanic theory has to be well optimised. The calculation performed in solid state physics and material science are based on the density functional theory (DFT), developed in the 60s [8–10]. DFT is a very powerful quantum mechanics method to study the electronic structure and properties of atoms in molecules and solids. With the recent development of cheap and powerful processors, interconnected with high speed network to form efficient massively parallel computers, the number of applications of ab initio calculations is increasing almost exponentially.

Let us just cite a few examples: in metallic materials, ab initio calculations have been widely used to study the properties of simple metals, ordered compounds such as intermetallics as well as carbides, hydrides and nitrides. The electronic structure of these materials has been studied in great length in particular the magnetic effects in Fe alloys such as Fe₄N (γ'), FeN_x ($0.2 < x < 0.5$) (ϵ) Fe₂N (ξ) and Fe₁₆N₂ (α'') [11–14], or the Invar and magneto-volume effects in FeNi ordered compounds [15].

Ab initio calculation in intermetallics have also been coupled to cluster expansion methods to obtain phase diagrams [16–20].

Point defects, as well as the effect of isolated substitute or foreign interstitial atoms in a metallic matrix have been much less studied. Most of the efforts so far have concentrated on the isolated vacancy.

As regard the study of interfaces, some groups have examined the problem of grain boundary segregation, for instance in the case of phosphorus in Fe [21–24]. However, because of the limited size of the supercell, the grain boundary selected has to have a short periodicity or to be a twin boundary.

In the field of plasticity, stacking fault energies, as well as generalised stacking fault energies have been calculated by ab initio in most of the pure metals. These data have been used in Peierls Nabarro models to predict the core structure and spreading of the dislocations. And only few works have considered direct calculation of the core structure of screw dislocations in bcc [25] or hcp metal where lattice friction is a key issue for the dislocation motion at low temperature.

Besides giving insight in the basic phenomena involved in the microstructure evolution, the data obtained by *ab initio* can be used as input data in larger scale models such as kinetic Monte Carlo models, as fitting properties in the building of empirical potentials [26] as well as checkpoints for the existing empirical potentials. The configurations of the atoms around a defect can also be used in higher scale models to help interpret experimental results such as positron annihilation results [27,28].

This paper presents *ab initio* calculations applied to metallic structural materials (pressure vessel steels and cladding materials) used in nuclear energy. The accessible quantities, the method and the definition of the different physical quantities are described in a first part. The results obtained in bcc Fe and hcp Zr matrix which are host structures for ferritic steels and zirconium alloys are then exposed. The different points discussed are the properties of intrinsic point defects, foreign interstitials, solute atoms, as well as stacking faults and dislocation core structure.

2. Electronic structure methods

In the field of materials science, two different approximations which lead to two different theories are behind *ab initio* calculations: the DFT and the Hartree–Fock (HF) theories. The HF theory is mainly used to treat molecular or cluster systems and will not be discussed in this paper, while DFT is more adapted for bulk or surface systems.

Ab initio calculations based on the density functional theory [8,9] have now demonstrated their capability to treat large enough number of atoms for investigating a broad field of problems in materials science (e.g. see the review of Hafner [29]).

2.1. *Ab initio* methods

The DFT is devoted to the determination of the electronic structure ground state. The fundamental statements are: (i) the total energy is a unique functional of the electron density; (ii) the minimum value of the total energy functional is the ground state of the system [8]; (iii) the many-electron Hamiltonian can be formally replaced by a set of self-consistent one-electron Hamiltonians [9].

In order to solve these Kohn–Sham one-electron equations, the wave-functions are represented by a linear combination of a finite number of basis functions, which have to be chosen in order to achieve

the optimal accuracy with the best computer efficiency. One can define four classes of basis set: (i) linear combinations of atomic orbitals (LCAO), (ii) linearised augmented plane waves (LAPW), (iii) linear combination of numerical orbitals (e.g. SIESTA code), (iv) and plane waves (PW) with pseudopotentials (e.g. VASP, PWSCF, ABINIT, CASTEP, ... codes).

The computational procedure described hereafter concerns the last class with the use of ultrasoft pseudopotential and plane wave basis set (see review paper [30]), but some features such as the size of the basis set or the sampling of the Brillouin zone are also important issues for localised orbital scheme.

Regarding the calculation of magnetic systems, such as ferritic materials, the standard methods treat the spin up and spin down electronic density with collinear spins. However non-collinear magnetism [31], which is much more complicated to model, has also been taken into account and introduced in the models to study pure phases for instance bulk γ -Fe [32], Cr [33] or Mn [34].

In the DFT, the exchange and correlation can be described with different approximations. The most simple one and most used one, the Local Density Approximation (LDA), considers the exchange and correlation energy to be the same as an homogeneous electron gas with the same density. Behind LDA, the Generalized Gradient Approximation (GGA) takes into account in addition the gradient of the density.

The DFT provides usually very good results, but has nevertheless some limitations. LDA and GGA can lead to different results, for example, in Fe, GGA predicts the right bcc ferromagnetic ground state, whereas LDA predicts instead the hexagonal non-magnetic structure as the most stable. Beside these differences, the DFT within the LDA or GGA are the most predictive for ground-state properties and non-correlated electron systems. For strongly correlated systems, encountered with some rare earth elements (with localised f orbitals) or some insulating transition-metal oxides (predicted metallic with the LDA, e.g. for NiO, UO₂) some refinement have been developed such as for example the LDA + U [35] or self-interaction correction methods [36]. In addition, the DFT usually does not do a very good job for the description of the conduction band which is not well reproduced compared to experiment and the gaps are usually underestimated. This leads to a bad description of the excited states. Some methods have been

developed to obtain the excited states: GW approximation [37] provides for instance a very good band structure for not too much correlated systems [38].

2.2. Physical properties and DFT limitations

The elementary physical properties are derived from the energy (or the derivatives of the energy) and the electronic structure of the system. Some of the physical properties which can be obtained are:

- the structural parameters (lattice parameters and relative co-ordinates),
- the structure stability (face centered cubic (fcc), body centered cubic (bcc), hexagonal close packed (hcp), ...),
- the point defect configurations (e.g. the relative stability of $\langle 110 \rangle$ and $\langle 111 \rangle$ self-interstitial configurations in bcc, or the tetrahedral versus octahedral configuration for foreign interstitials),
- the formation and binding energies (e.g. vacancy formation energies, vacancy-solute binding energies),
- the migration energies (vacancy or interstitial migration energies), or more precisely the activation barriers for the defect to move from one site to another,
- the vibrational properties (phonons),
- the elastic constants and the bulk modulus,
- the stacking fault energies,
- the density of states and band structure,
- the chemical bonding (e.g. the covalent or ionic character),
- the magnetic properties (e.g. the ferro or anti-ferromagnetic configurations, the local magnetic moments around a defect).

From the elementary properties different problems can be tackled.

In bulk, diffusion properties can be determined: self-diffusion, solute or impurity atom diffusion, as well as point defect diffusion. Indeed the diffusion coefficients can be obtained from the calculation of the activation barriers, and the vibrational modes of the diffusive specie based on Vineyard theory [39]. The mobility of small defect clusters or mixed solute/foreign interstitial defect clusters is also an important quantity which may be determined but more complex to determine. In addition binding energies between entities constituting these clusters is in particular related to their lifetime and are therefore important to know.

The dislocation core structure and its deformation under stress can be obtained, despite the small system size tractable. In addition, some insights on the influence of impurities or foreign atoms on the dislocation structure can be obtained through the evolution of the stacking fault energy.

Interfaces (grain boundaries, metal oxide interfaces if the lattice mismatch is small enough) cohesion properties, as well as species segregation can be evaluated. Surface properties such as, surface relaxation and/or reconstruction, specie adsorption or chemisorption, specie diffusion can also be addressed.

The precise evaluation of the accuracy of the energies obtained is rather difficult and depends on the quantities calculated. For example, the error on the lattice parameters is usually a few percent, while the uncertainty on point defect binding energies in transition metals can be evaluated to be of the order of 0.1 eV, but this depends on the methodology.

2.3. Computational procedure

Our calculations have been performed using the Vienna Ab initio Simulation Package VASP [40,41]. The calculations were performed in a plane wave basis, using fully non-local Vanderbilt-type ultrasoft pseudopotentials (USPP) to describe the electron-ion interaction [42,43]. Exchange and correlation were described by the Perdew and Zunger functional [36], adding non-local correction in the form of the GGA of Perdew and Wang [44]. The ultrasoft pseudopotentials were taken from the VASP library. In addition, when mentioned specifically (for He in Fe, Cr and Ni specially), some calculations were done using the Projector Augmented Wave (PAW) approach [45,46].

The supercell approach with periodic boundary conditions was used to simulate point defects as well as pure phases. Brillouin zone sampling was performed using the Monkhorst and Pack scheme [47]. The ion relaxations were performed using the standard conjugate gradient algorithm implemented in the VASP code. Most of the calculations were done at constant volume thus relaxing only the atomic position in a supercell dimensioned with the equilibrium lattice parameter for Fe or Zr. This allows one to use a smaller plane wave energy cutoff from 240 eV up to 350 eV depending on the impurities considered in our system (see Appendix A). The relative error induced by this lower energy cutoff

was checked to be negligible, as can be seen later in text and in our previous work [48]. For some calculations, when specified, the volume has also been relaxed in order to minimise the stress tensor. In all the results presented here, the number of k points is the total number of k points (not the number of irreducible k points which depends on the supercell symmetry). A discussion on the convergence of the results with the number of k points can be found in [48]. In all the tables presented below, the ‘number of atoms’ is more precisely the number of metal sites in the perfect supercell, i.e. the cell without any defects. Additional technical details can be found in Appendix A.

The relaxation of the volume is converged when the pressure or stress tensor on the supercell is zero, as usually done in other literature ab initio calculations. For constant volume calculations, some stresses remain on the supercell which can become high for small supercells with point defects or point defect clusters with a large formation volume. The values obtained by these two methods should bracket the correct answer. However the realistic defect concentrations may be obtained by putting one defect in an ‘infinite’ crystal (from our ab initio supercell angle). At the surface of this crystal the stress tensor is zero, whereas at the boundary of our supercell the right stress (which is not zero) is given by the elastic response of the crystal. This stress defines the equilibrium volume of the supercell with the defect. Such method can be implemented using Green’s functions and it has been applied for dislocation core structure studies [49]. This method may give values in between the two previous ones. However, for point defect properties,

constant volume and relaxed volume lead to energy differences smaller or equal to other values from the literature obtained with other codes and/or other pseudopotentials as shown in this paper in paragraph 3.1 hereafter.

2.4. Computational method and analysis

The binding energies between two entities in a bcc iron or hcp zirconium matrix are calculated as follows. The binding energy $E_b(A_1, A_2)$ is defined as the difference of two system energies $E(\text{non-interact})$ and $E(\text{interact})$: $E_b(A_1, A_2) = E(\text{non-interact}) - E(\text{interact})$.

In system ‘non-interact’, A_1 and A_2 do not interact, i.e. they are situated far enough from each other not to interact. In system ‘interact’, A_1 and A_2 interact, and the distance between A_1 and A_2 may be first nearest neighbour distance, second nearest distance and so on (Fig. 1).

Because of the relatively small supercell sizes one may use, it is rather difficult to make sure that the two entities in system ‘non-interact’ do not interact even when they are as far as the supercell size allows. Another method can be used to determine the binding energies which consists in subtracting from the energy of system ‘interact’ (where A_1 and A_2 interact), the energy of a system containing A_1 (calculated with a supercell with a size similar to that of system ‘interact’) as well as that of a system containing A_2 (obtained with similar conditions) and that of the supercell with neither A_1 nor A_2 (Fig. 1).

For a supercell containing N atoms, the binding energy is thus obtained as

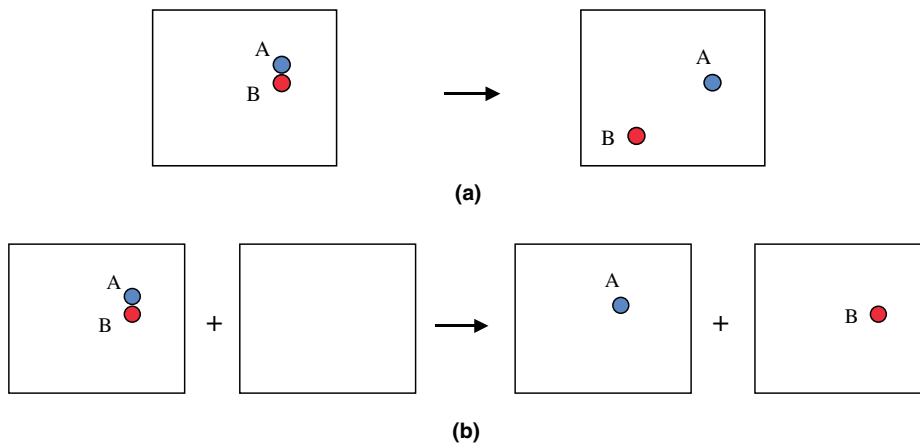


Fig. 1. Point defect binding energy determination (a) direct calculation, (b) indirect calculation for small system size.

$$E_b(A_1, A_2) = [E(A_1) + E(A_2)] - [E(A_1 + A_2) + E_{\text{ref}}], \quad (1)$$

where E_{ref} is the energy of the supercell without A_1 and A_2 , $E(A_1)$ (respectively $E(A_2)$) is the energy of the supercell with A_1 (respectively A_2), $E(A_1 + A_2)$ is the energy of the cell containing both A_1 and A_2 interacting, i.e. the energy of system ‘interact’ in the previous method. All the supercells contain the same number of sites, i.e. have the same size.

For more than two interacting entities, Eq. (1) can be generalised as follows:

$$E_b(A_1, \dots, A_{n2}) = \sum_i E(A_i) - [E(A_1 + \dots + A_n) + (n - 1)E_{\text{ref}}]. \quad (2)$$

For the solid solutions in a matrix of X element, the heat of solution or formation enthalpy is calculated when the solute is in substitution

$$E_{\text{for}}(\text{sub}) = [E((N - 1)X + A) - ((N - 1)/N)E_{\text{ref}} - E(A_{\text{ref}})]. \quad (3)$$

When the solute is in an interstitial position

$$E_{\text{for}}(\text{int}) = [E(NX + A) - E_{\text{ref}} - E(A_{\text{ref}})], \quad (4)$$

where $E((N - 1)X + A)$ is the energy of a supercell containing $(N - 1)X$ atoms and one solute atom A , $E(NX + A)$ is the energy of a supercell containing NX atoms and one solute atom A , E_{ref} is the energy of a supercell containing NX atoms and $E(A_{\text{ref}})$ is the energy of solute A in the reference state chosen.

The electronic structure can be analysed using the density of states as well as the electronic density deformation map. For a supercell $(A_n X_i)$ containing nA atoms and iX atoms, the electronic density deformation map due to the presence of atoms of type X is obtained by subtracting from the electronic density of $(A_n X_i)$ both the electronic density of (A_n) and the electronic density contribution of each isolated (X_k)

$$\Delta\rho = \rho(A_n X_i) - \rho(A_n) - \sum_{k=1,i} \rho(X_k \text{ isolated}), \quad (5)$$

(A_n) is the supercell where all the X atoms have been removed, and (X_k) is isolated in the same supercell. In this scheme, isosurfaces of the deformation map give a direct real space visualisation of the local electronic rearrangements due to the presence of the X atom(s).

To calculate the excess stacking fault energy for a given fault plane and a given vector, a rigid translation of two crystal blocks surrounding the fault

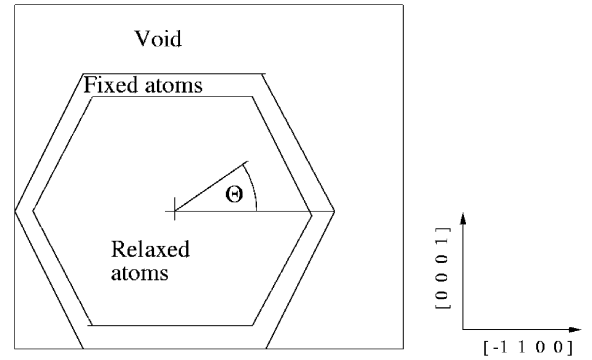


Fig. 2. Schematics of the supercell used to simulate screw dislocation cores.

plane is applied. The atoms are relaxed only in the direction perpendicular to the fault plane until the forces are smaller than 0.02 eV/\AA . Free surfaces parallel to the fault plane and periodic boundary conditions in the remaining directions were used in order to investigate all possible fault planes and translation vectors [50].

To simulate an $\langle a \rangle$ screw dislocation in hcp, the line is placed at the centre of a supercell containing a stacking of two $(2\bar{1}10)$ atomic planes. An initial atomic displacement field derived from linear isotropic elasticity is then applied. The atoms are then relaxed except those located far from the line that are kept fixed, surrounded by a vacuum ribbon (see Fig. 2). A periodic boundary condition is applied along the dislocation line. The relaxed dislocation core is analysed using the arrow method developed by Vitek [51].

3. Point defects

3.1. Intrinsic point defects

The intrinsic point defects (vacancies and self-interstitials), can have different configurations depending on the crystal structure. The relative stability of the self-interstitial configurations in a given material is an important issue influencing their mobility within the material and their ability to contribute to the solute diffusion. To get accurate experimental value of their formation and migration energy is a very difficult task. The calculation of the formation energies using ab initio calculations constitute an important added value, as previously only empirical potentials fitted on some equilibrium properties were able to provide such data.

Table 1
Vacancy and self-interstitial formation energies in bcc Fe (in eV)

System	System size	E_{vac}^f	O	T	$\langle 100 \rangle$	$\langle 110 \rangle$	$\langle 111 \rangle$	$\Delta E_{\langle 111 \rangle - \langle 110 \rangle}$
GGA VASP	54 at. Full rlx	1.95			4.37	3.41	4.11	0.7
GGA VASP	54 at. Cst vol	1.93	5.35	4.53	5.07	3.96	4.75	0.79
GGA VASP	128 at. Cst vol	2.02		4.46	5.04	3.94	4.66	0.72
GGA SIESTA [56]	128 at. Full rlx	2.07	4.94	4.26	4.64	3.64	4.34	0.70
EAM [61]					4.57	3.67	3.54	-0.13
FS [62]			6.03	5.66	–	4.87	5.00	0.13
EAM [26,90]		1.84	4.19	4.16	4.34	3.53	4.02	0.5

'Full rlx' indicates that the supercell is relaxed in order to get a null stress tensor, whereas 'Cst vol' means that only the atomic positions are relaxed. O means octahedral position, T means tetrahedral position. The calculations done with 54 atom supercells by 125 k points and those done with 128 atom supercells by 27 k points.

The vacancy formation energy and other related properties have been studied by ab initio in various metals [52–55]. However, very few works have been devoted to ab initio calculations of self-interstitials: [48,56] in Fe, [57,58] in Zr, [59] in Mo and V.

We have examined some properties of the vacancy and self-interstitial atom in α -Fe [48]. The different defect energies for various configurations are gathered in Table 1. The vacancy formation energy was found to be 2.02 eV. The binding energy between two vacancies is the largest when they are in second nearest neighbour position. These first principle calculations have confirmed that the self-interstitial atom the most stable is a $\langle 110 \rangle$ dumbbell in agreement with experiments. It was found that a large formation energy difference of 0.7 eV exists between the $\langle 110 \rangle$ and $\langle 111 \rangle$ configurations ($E_{\text{for}}^{(110)} = 3.94$ eV and $E_{\text{for}}^{(111)} = 4.66$ eV). These results confirm previous calculations of Johnson [60], but they disagree with most of the embedded atom method (EAM) empirical potentials [61,62]. In addition some recent ab initio calculations have confirmed that the migration energy of the $\langle 110 \rangle$ dumbbell is 0.3 eV [56] in agreement with experimental measurements and with previous simulations of Johnson [60]. Furthermore, in order to evaluate the effect of the supercell size, the vacancy and

dumbbell formation energies have been determined for different system from 54 up to 2000 atoms at constant volume to follow the same ab initio method we have adopted (Table 2). If ones define the error as the difference between 54 (resp. 128) atom supercell calculation and large supercell, the error is around 0.1–0.15 eV (resp. 0.05 eV) for interstitial and 0.03 eV for vacancy.

The ab initio calculations of point defects in hcp Zr, have also shown some differences compared to the prediction of existing empirical potentials [63,64] (Table 3). The vacancy formation energy (1.86 eV) agrees with previous calculations made using empirical potentials and with the available experimental estimations. Concerning self-interstitial atoms the octahedral configuration has the lowest formation energy $E_{\text{O}}^f = 2.84$ eV, but the basal octahedral and the basal crowdion have formation energy very close to E_{O}^f (2.88 and 2.95 eV, respectively). Among the different interstitial configurations, five different SIA configurations have formation energies within 0.24 eV indicating possible polymorphism. Our ab initio results are in good agreement with other GGA calculations [58].

In addition, the energy difference between constant volume and fully relaxed configuration is almost equal for most of the configurations to the

Table 2
Vacancy and dumbbell formation energies in bcc Fe (in eV)

System size (# unit cells)	System size (# atoms)	E_{vac}^f (ab initio)	E_{vac}^f (EAM)	$E_{\langle 110 \rangle}^f$ (ab initio)	$E_{\langle 110 \rangle}^f$ (EAM)
$3 \times 3 \times 3$	54	1.93	1.729	3.96	3.646
$4 \times 4 \times 4$	128	2.02	1.723	3.94	3.557
$6 \times 6 \times 6$	423		1.720		3.533
$8 \times 8 \times 8$	1024		1.717		3.527
$10 \times 10 \times 10$	2000		1.713		3.524

Effect of the supercell and evolution of the formation energy for large system size using the recent EAM potential derived by Ackland et al. [90].

Table 3
Vacancy and self-interstitial formation energies in hcp Zr (in eV)

	System size	Vac	O	Bo	Bc/Bs	C	S	Bt
GGA	96 cst vol	1.86	2.94	2.98	3.09	3.25	3.12	4.14
GGA	96 full rlx	1.86	2.84	2.88	2.95	3.08	3.01	4.03
LDA [58]	36		2.73	2.97	3.23	3.18	2.95	
	96		2.79	2.78	2.90	3.07	2.80	
GGA [58]	36		3.04	3.14	3.39	3.52	3.28	
Emp. [63]		1.79	Bo	3.97	3.76	3.98	4.32	Bo
Emp. [64]		1.74	2.80	2.63	2.50	2.78	3.04	2.80

The calculations done with 96 atom supercells were sampled by 48 k points.

elastic contribution to the relaxation energy [57], and the energy difference represents about 0.1 eV for 96 atom supercells.

The propensity of elementary point defects to form vacancy or interstitial clusters is also important under irradiation, and their properties in term of stability and mobility play an important role in the evolution of the system. The study of small vacancy [65] and interstitial [66] clusters, and in particular the determination of the binding energies has also started in Fe despite the small supercell size considered (indeed relaxation effects may become important for large self-interstitial clusters).

The ab initio calculations of self-interstitials in Fe and Zr has thus provided new figures and relative stabilities. In the case of Fe, the use of these ab initio data have allowed to build new empirical potentials in Fe with self-interstitial properties in better agreement with experimental data. Recently some new Fe EAM potentials have been derived using our ab initio interstitial formation energies which predict correctly the stability of the $\langle 110 \rangle$ dumbbell [26].

For pure Fe, the ab initio data have been recently used to simulate isochronal annealing by event kinetic Monte Carlo [67] or the long term evolution of neutron irradiation by object kinetic Monte Carlo [68].

3.2. Extrinsic point defects

Extrinsic point defect can be classified into foreign interstitial atoms which are atoms much smaller than the host element and substitutional atoms.

3.2.1. Foreign interstitial defects

The foreign interstitials most commonly encountered are H, C, N, O in as received metals and He under irradiation. Helium is a rare gas and has a particular behaviour due to its filled shell.

Table 4 summarises the heats of solution determined using Eq. (3) when the impurity atoms (H, C or N) are positioned in different possible configurations in a bcc Fe matrix. In that case, the heats of solution are relative to the reference state chosen: the isolated C, N or H atoms. As expected, the behaviour of these three elements is not similar.

For both C and N, the most stable position in the α -Fe matrix is the octahedral (O) site in agreement with the most common interpretation of the experimental observations by internal friction, Mossbauer spectroscopy of FeC and FeN martensite [69] and simulations by Johnson et al. [70] and Rosato [71] using empirical potentials. Furthermore, for these two elements, the tetragonal site is a saddle point for the migration in α -Fe. Consequently, $\Delta E(T) -$

Table 4

Heat of solution E_{for} (Eqs. (3) and (4)) (eV) of and relaxation (in % of $\Delta d_1/d_1^0$) around a single C or N atom positioned in the two interstitial sites, in a substitutional configuration

Configuration	C (54 at.)	$\Delta d_1/d_1^0$	C (128 at.)	N (54 at.)	$\Delta d_1/d_1^0$	N (128 at.)	H (54 at.)	$\Delta d_1/d_1^0$
Substitutional	-8.742	-5.0	-8.094	-2.387	-4.3	-2.219		
Tetrahedral	-9.787	+13.7	-9.557	-4.407	+11.9	-4.342	0.162	+4.6
Octahedral	-10.710	+23.8	-10.459	-5.196	+22.9	-5.107	0.308	+11.5
$\Delta E(T) - (O)$	0.923		0.902	0.789		0.765	0.15	
E_{mig} (eV) experimental	0.82 eV [72]–0.88 eV [79]			0.78 eV [72]–0.81 eV [105]			0.1–0.2 [74]	

The reference state is the isolated C and N atom, and the H₂ molecule. Calculations made with 54 atom supercells sampled by 125 k points.

(O)) is the C or N migration energy. The results obtained in these calculations, reported in Table 4, are in very good agreement with the experimental data. More over, Weller [72] observed that upon irradiation of α -Fe, the interstitial carbon stays in solution to a somewhat higher temperature than nitrogen. This fact is consistent with the migration energy being higher for C than for N.

For H on the other hand, the tetrahedral configuration is the most stable configuration, in agreement with the experimental data [73]. If one assumes that the path of the H atom for diffusion between two tetrahedral sites is less or equal to the one through the octahedral site, then the migration energy for H is very low and less or equal to 0.15 eV in very good agreement with the experimental data gathered in Landolt and Börnstein [74] which most of the time indicates a low migration energy around 0.1 or 0.2 eV.

The diffusion coefficient can be directly calculated from the migration energies and from the attempt frequencies. These frequencies are linked to the dynamical matrix and to the vibrational modes of the atoms which can be determined by ab initio through the Vineyard theory. As the determination of the whole dynamical matrix requires numerous calculations, the calculations are

restricted to the vibrational mode of the migrating species in the framework of the Einstein approximation. Using this method, we found that the diffusion coefficient of C in bcc Fe [7], that of N in bcc Fe [7], and that of H in Zr [75] are in close agreement with the experimental measurements (Table 5). The C diffusion coefficient is in agreement with Jiang and Carter [76] ab initio calculations.

In addition, from previous works, the analysis of the density of states of C and N in Fe [7] as well as that of H in Zr [77], shows that the hybridisation between the FIA valence electrons and the 3 d electrons are localised a few eV below the Fermi level.

Table 6 summarises the binding energies of a C, N or H atom in first and second nearest neighbour position to a single vacancy. Our results indicate that a foreign interstitial atom near a vacancy does not become ‘substitutional’ and that the distance between the FIA and vacancy does not vanish. The data obtained here are in good agreement with the experimental data available. For C, they are also in agreement with the results obtained by Johnson et al. [70] or Rosato [71] from empirical potentials. One must stress out that the experimental results are not always very clear and are extracted using different techniques. On the one hand, Arndt and Damask [78] find a binding energy of C with a

Table 5

FIA diffusion coefficient $D_0 \exp(-E_a/kT)$ determined from ab initio compared to experimental measurements for C and N in bcc Fe, and H in hcp Zr, and to literature ab initio calculations for C in Fe

	Ab initio	Exp.
C in Fe	$D_C^{\text{Fe}} = 2.3 \times 10^{-7} \exp\left(\frac{0.92}{kT}\right) \text{ m}^2 \text{ s}^{-1}$	$D_0 = 4.88\text{--}7.8 \times 10^{-7} \text{ m}^2 \text{ s}^{-1}$ [106] $E_a = 0.82 \text{ eV}$ [72] $E_a = 0.88 \text{ eV}$ [79]
N in Fe	$D_C^{\text{Fe}} = 1.44 \times 10^{-7} \exp\left(\frac{0.86}{kT}\right) \text{ m}^2 \text{ s}^{-1}$ [76] $D_N^{\text{Fe}} = 0.94 \times 10^{-7} \exp\left(\frac{0.79}{kT}\right) \text{ m}^2 \text{ s}^{-1}$	$D_0 = 1.67\text{--}3.94 \times 10^{-7} \text{ m}^2 \text{ s}^{-1}$ [106] $E_a = 0.78 \text{ eV}$ [72] $E_a = 0.81 \text{ eV}$ [105]
H in Zr	$D_H^{\text{Zr}} // = 6.7 \times 10^{-7} \exp\left(-\frac{0.40}{kT}\right) \text{ m}^2 \text{ s}^{-1}$ $D_H^{\text{Zr}} \perp = 4.1 \times 10^{-7} \exp\left(-\frac{0.39}{kT}\right) \text{ m}^2 \text{ s}^{-1}$	$D_H^{\text{Zr}} // = 3.4 \times 10^{-8} \exp\left(-\frac{0.42}{kT}\right) \text{ m}^2 \text{ s}^{-1}$ $D_H^{\text{Zr}} \perp = 1.73 \times 10^{-7} \exp\left(-\frac{0.39}{kT}\right) \text{ m}^2 \text{ s}^{-1}$ [107]

Table 6

Vacancy – FIA binding energies (in eV) and distance to vacancy (in a_0)

Configuration	$E_b\text{C}$ (eV)	$d_{\text{C-V}}$ (a_0)	$E_b\text{N}$ (eV)	$d_{\text{N-V}}$ (a_0)	$E_b\text{H}$ (eV)	$d_{\text{H-V}}$ (a_0)
Vacancy 1st nn	0.44	0.40	0.67	0.45	0.51	0.40
Vacancy 2nd nn	–0.09	0.64	0.14	0.72		
Exp. results	0.41–1.1 (see text for details)	0.365 [81]	0.14		0.63 [73]	

The V-C binding energy (in first neighbour position) obtained with empirical potentials are 0.41 eV for Johnson et al. [70] and 0.48 eV for Rosato [71]. Calculations made with 54 atom supercells sampled by 125 k points.

defect of 0.41 eV which they interpret to be a vacancy. However, some other experimental works suggest interaction with interstitial clusters which may correspond to some higher binding energies 1.1 eV by Takaki et al. [79] or 0.85 eV by Vehanen et al. [80]. In addition, the C–V relaxed distance obtained is in good agreement with the experimental data [81].

This work indicates that the vacancy-FIA binding energy is indeed very high. As a consequence, the formation of C-vacancy, N-vacancy or H-vacancy complexes can explain the difficulty to obtain coherent experimental data on vacancy properties. Several FIA can be associated to a vacancy. The total binding energy of a vacancy with up to four FIA (C or N only) are given in Table 7. Only the most stable configuration is presented for each case. The different behaviour of C and N as far as which configuration is the most stable in each case is due to the interaction of the FIA with its Fe neighbours as well as with its FIA neighbours. Indeed the binding energies with the vacancy are higher for C than for N, as the repulsion between two C atoms is smaller for C than for N. In particular, the V-C₂ configuration leads to the formation of a C–C covalent bond which can be clearly displayed by analysing the changes in the electronic density. Indeed, the electronic deformation map in the (100) plane containing the two FIA and the vacancy shown Fig. 3 clearly underlines the

different interaction involved when the FIAs are C or N.

He is also a small atom, but because it is a rare gas, its behaviour in metals is different from that of C or N. Some elementary properties of He in different transition metals (Fe, Ni and Cr) have been calculated and compared in Table 8.

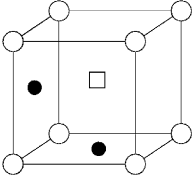
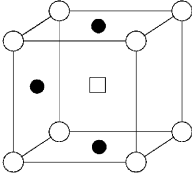
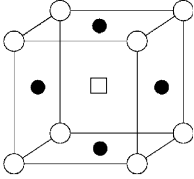
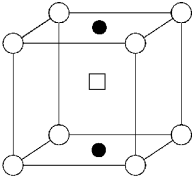
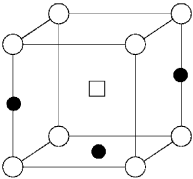
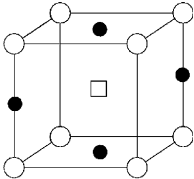
Despite its size, He occupies preferentially the substitutional position. The most favourable interstitial configuration is the tetrahedral one, with a low energy difference compared to the octahedral site. The same behaviour is observed in several metals Fe, Cr and Ni. Our results are in agreement with other recent ab initio calculations in Fe [82]. The results presented in Table 8 represent a first step towards the study of the interaction of He with point defects and with other He atoms in FeCrNi alloys to model swelling of austenitic steels.

In addition, under irradiation with He production, the He formed can be trapped by the vacancies present in the matrix and lead to the formation of He bubbles [83,84]. Our ab initio calculations, in agreement with results obtained with an empirical potential, show that several He atoms can be trapped per vacancy [85].

3.2.2. Substitutional atoms: interactions with vacancies

Different atomic species (Cu, Ni, Mn, Cr, Si, P, W and Mo) which can be found in ferritic steels

Table 7
Vacancy – FIA cluster binding energies (in eV)

Configuration	V-2FIA	V-3FIA	V-4FIA
C	 1.24	 1.24	 0.54
E_b (eV)			
N	 1.25	 -0.08	 0.13
E_b (eV)			

Calculations made with 54 atom supercells sampled by 125 *k* points.

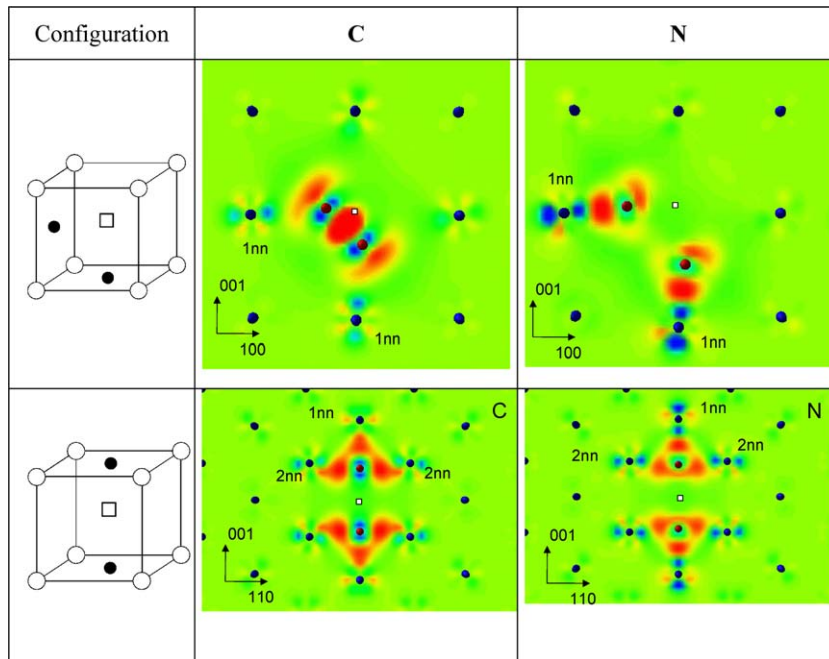


Fig. 3. Electronic density charge deformation map. The red color indicates an increase of the electronic density, the blue color a decrease of the electronic density. (For interpretation of the references in color in this figure legend, the reader is referred to the web version of this article.)

Table 8

He relative stability (in eV) in Fe, Cr and Ni

	Fe bcc	Cr bcc (NM)	Ni fcc
He subs	0	0	0
He (O)	0.57	0.43	1.39
He (T)	0.36	0.23	1.27
E_{for} (SIA)	4.10	5.65	4.80

Calculations made with 54 atom (for Fe and Cr) and 32 atom (for Ni) supercells sampled by 125 k points.

have been studied. Because of their size, they are in substitution in the Fe matrix. Among them, Cu, Ni, Mn, Cr have a size rather similar to that of the atoms of the host matrix, whereas Si, P are under-

sized solutes and W and Mo are oversized. The interaction with point defects such as vacancies will depend on the relative size of the solute atom compared to Fe as well as on the chemical interactions, which should be predominant when the sizes are similar.

We have extensively studied solid solutions of those of the solute atoms Cu, Ni, Mn, Si and P [86–88] which are supposed to influence the embrittlement under irradiation of the pressure vessel steels. The other solutes have been, for the time being, less investigated. In our calculations, the creation of this so-called ‘solid solution’ consists in substituting one Fe atom by a solute atom in a 54 atom supercell (sometimes 128 atom supercell).

Table 9

Heat of solution E_{for} (Eq. (3)) (in eV) and relaxation of the three first neighbour shells around the solute atom (in % of the non-relaxed distance)

Configuration	Cu	Ni	Mn	Si	Cr	P
ΔH (eV)	0.55	−0.22	−0.14	−1.12	−0.35	−4.53
First nearest neighbour	0.92	0.20	0.43	−0.19	−0.23	−0.9
Second nearest neighbour	−0.23	−0.13	−0.26	−0.71	0.06	−0.03
Third nearest neighbour	−0.13	0.09	−0.02	0.05	0.04	−0.2

The reference state for the solute is its ground state bulk phase (i.e. fcc Cu, bcc Cr, fcc Ni, bcc Mn, diamond Si) except for P where the reference state is the isolated atom. Calculations made with 54 atom supercells sampled by 125 k points.

The heat of solution E_{for} (Eq. (3)) and the relaxation of the first and second nearest Fe atoms surrounding the solute atoms are presented Table 9. As expected from the experimental phase diagrams, Cu has a positive heat of solution (or solution enthalpy), whereas E_{for} is negative for Ni, Mn, Si, Cr and P. The values obtained in Table 9 are in agreement with the solute solubility limit trends: the solubility limit of Cu in α -Fe is very low, whereas Si, Ni, Cr, Mn and P have a rather high solubility limit [86].

Interactions between a solute atom and a vacancy (in a first and second nearest neighbour position) have been determined. The binding energy values obtained using Eq. (1) are reported in Table 10. Cu, Si and P have a positive binding energy in

first and second nearest neighbour position, while Ni is positively bound to the vacancy in second nearest position only. No significant tendency is obtained for Mn, whereas Cr does not seem to interact with the vacancy. These results are in very good agreement with the muon spin rotation experiments of Möslang et al. [89] who observe an important binding between the vacancy and Cu, Ni or Si, and no binding energy or a binding energy below the experimental resolution of the vacancy with Mn and Cr. For big oversize solutes such as Mo, W or Au, the interactions are large but are necessarily attractive. For Mo and W, in second nearest neighbour position, the repulsion is large. The electronic structure effects seem thus to be significant.

These interactions and binding energies can be used to build simple cohesive model to define an Hamiltonian for a multi-component alloy. This kind of data have been used to parameterise atomic kinetic Monte Carlo aiming at simulating the evolution of solute atoms in bcc Fe in presence of vacancies [87].

Table 10
Solute vacancy interaction in bcc Fe. Solute migration energy (in eV)

Element	E_{mig}	E_b V–X (1 nn)	E_b V–X (2 nn)	E_b (Exp.)
Fe	0.65	–	–	
Si	0.44	0.23	0.15	0.21 [89]
P	0.34	0.31	0.26	
V	0.57	0.03	–0.10	
Cr	0.58	0.03	0.00	◇ [89]
Mn	1.02	0.09	–0.08	◇ [89]
Co	0.72	–0.06	0.10	
Ni	0.70	0.03	0.19	0.21 [89]
Cu	0.56	0.17	0.21	0.11 [89] 0.14 [108]
Mo	0.57	0.08	–0.20	
W	0.79	0.06	–0.17	
Au	0.76	0.33	0.19	

Vacancy-solute binding energy in first (1nn) and second (2nn) nearest neighbour position (in eV). Calculations made with 54 atom supercells sampled by 125 k points. A ◇ sign in the experimental binding energy indicates that it is less than 100 meV according to Möslang and coworkers [89].

3.2.3. Substitutional atoms: interactions with self-interstitial atoms

P in Fe and Nb in Zr are both substitutional solute, but they have a size significantly smaller than the atom of their host matrix. Their interaction with self-interstitial atoms can thus be potentially significant because of size as well as chemical effects.

For phosphorus, among the different possible configurations, it was found that the most stable configuration is the mixed $\langle 110 \rangle$ dumbbell with a formation energy of 2.92 eV (using Eq. (4)) (Table 11). The ab initio data of Table 11 are in good agreement with those obtained with a recently developed EAM potential based on ab initio calculations [90]. The almost 3 eV energy difference

Table 11
P occupation site in bcc Fe

	EAM [90]	Ab initio [90] 16 atoms	16 atoms	54 atoms	128 atoms
Substitution	0	0	0	0	0
Tetrahedral	2.8	4.35	4.35	3.24	–
Octahedral	3.47		4.75	3.13	2.97
Mixed $\langle 100 \rangle$	Decays to mixed $\langle 110 \rangle$	4.75		Decays to (O)	Decays to (O)
Mixed $\langle 110 \rangle$	2.57	3.82	3.83	2.98	2.92
Mixed $\langle 111 \rangle$	3.30	4.36	4.35	3.40	3.25

The reference state for the energies (in eV) are the substitutional position for P and bcc Fe for Fe. The calculations done with 16 atom supercells were sampled with 343 k points, those done with 54 atom supercells by 125 k points and those done with 128 atom supercells by 27 k points. Our results are compared to ab initio (with 16 atoms) and EAM calculations (with 2000 atoms) obtained by Ackland et al. [90].

between the substitutional position and the mixed dumbbell induces a binding energy between a P in substitution and a $\langle 110 \rangle$ Fe dumbbell close to 1 eV as the formation energy of the $\langle 110 \rangle$ Fe dumbbell $E_{\text{for}}^{(110)}$ equals 3.94 eV (Table 12). One can notice that the binding energy of the mixed dumbbell is almost independent of the supercell size, and 16 atom supercell calculations [90] already lead to 1.00 eV. This small dependence of these relative values with the supercell size can be understood by the similar number of atoms and stress on the different supercells used to get this binding energy. Thus, when a self-interstitial comes close to a substitutional P, a mixed dumbbell is easily formed. Consequently, the trapping of self-interstitials by P and/or P transport by interstitial mechanism appears to be possible. In addition, P positioned in first nearest neighbour to the dumbbell leads also to a strong binding energy in the site in compression, whereas the site in tension is unfavourable (Table 13).

For Niobium, the most stable interstitial configuration is (O). The energy difference between substitutional and interstitial position is 2.15 eV, which is 0.68 eV lower than the self-interstitial formation energy (for a 36 atom supercell) and leads to a binding energy between a Nb and a SIA of 0.68 eV (Table 12). This high binding energy is in agreement with the small size of Nb as compared to Zr: the atomic volume of hcp Zr is 23.4 \AA^3 , whereas the one of bcc Nb (resp. hcp Nb) is 19.4 \AA^3 (resp. 19.0 \AA^3).

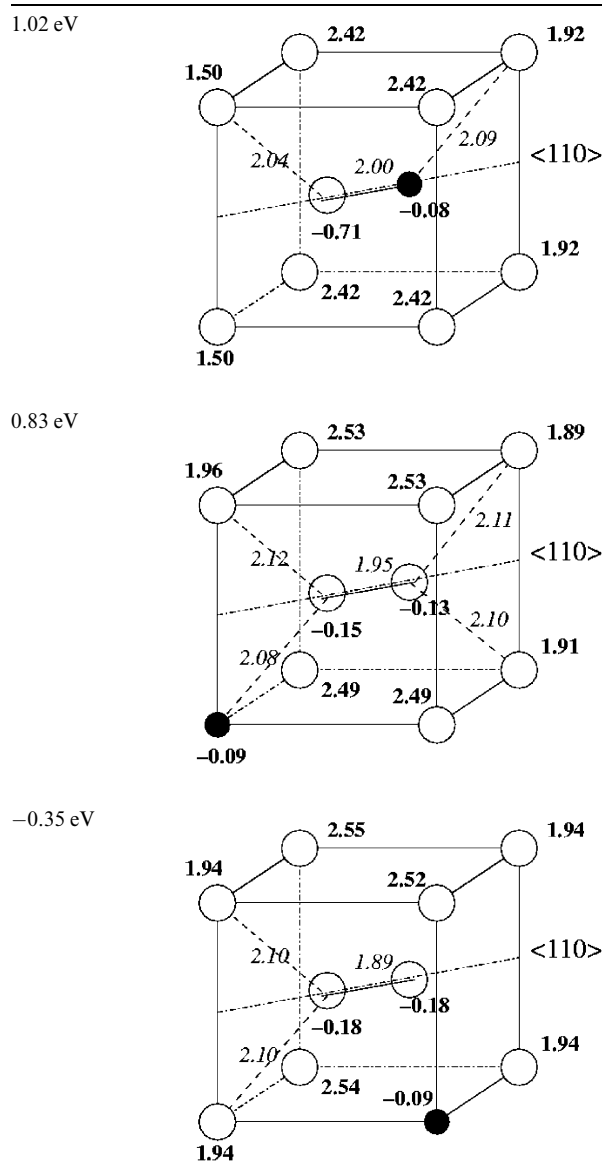
To summarise, both P in Fe and Nb in Zr strongly interact with self-interstitials, the interaction energy is around 0.6–1 eV. Despite the difficulty to separate the elastic contribution due to size effect

Table 12
Solute-SIA interaction energies (eV): P in bcc Fe and Nb in hcp Zr

	P in Fe [90] (16 atom supercell)	P in Fe	Nb in Zr
E_{for} (X subs)	0	0	0.61
E_{for} (X interstitial)	3.82	2.98	2.76
E_{b} (X/FIA)	1.00	0.96	0.68

The reference state is the substitutional position for P and the bulk bcc for Nb. The formation energy of the $\langle 110 \rangle$ self-interstitial atom in Fe is 3.94 eV. The formation energy of the (O) self-interstitial atom in Zr is 2.84 eV. The energies are given in eV. Calculations made with 54 atom (resp. 36 atom) supercells sampled by 125 k points (resp. 96 k points) for Fe (resp. Zr). By ab initio calculation on 16 atom supercell at constant volume, Ackland et al. [89] obtained 4.82 eV for the dumbbell formation energy.

Table 13
SIA – P binding energies (in eV) in bcc Fe



The P atom is the black circle. The local magnetic moment on the nearest neighbour atoms is in bold and the distance in Å. Calculations made with 54 atom supercells sampled by 125 k points. The reference state is the substitutional position for P and the $\langle 110 \rangle$ Fe self-interstitial atom.

and the chemical interaction, such large values indicate that the size effect is rather significant. Under irradiation, as soon as a self-interstitial atom in Fe or Zr migrates close to a P or Nb substituted atom, the P or Nb will move to an interstitial configuration. The possible diffusion of these defects is under study.

4. Extended defects

4.1. Stacking faults

We have studied stacking faults and generalised stacking faults in Zr, and to a less extent in Ti. In addition, we have also evaluated the influence of chemical impurities such as H on the stacking fault energy in Zr. Stacking fault energies represent useful data related to the preferential planes for dislocation core dissociation. They are easier to calculate than the core structure itself. In the case of hcp Zr and Ti, most of the empirical potentials predict a lower basal stacking fault energy compared to the prismatic one. This is in disagreement with the experimentally known screw dislocation motion which takes place in prismatic planes. Only the tight binding (TB) calculation of Legrand [91] gave a lower prismatic stacking fault energy.

The calculated values of the basal and prismatic stacking fault excess energies (Table 14) are in qualitative agreement with the tight binding calculations, the basal stacking fault energy (Zr: 200 mJ/m², Ti: 291 mJ/m²) being larger than the prismatic one (Zr: 145 mJ/m², Ti: 174 mJ/m²). Atomic relaxations are essential to obtain the γ_{pris} value while their effect is less pronounced to obtain γ_{bas} (they account for only 15% of the value). In addition, we have observed [92] that Zr or Ti pseudopotentials with semi-core p electrons leads to similar results for stacking fault energies (within 10% and 20% for basal and prismatic faults respectively) and elastic constants.

Our results are in agreement with the only available experimental value of 150 mJ/m² evaluated for Ti [93] for the stacking fault energy. Assuming a dislocation core dissociation in two partials, the previous results entail a preferential prismatic spreading.

Beside the stable stacking fault energy, we calculated the gamma-surface excess energy path along

the Burgers vectors $\langle a \rangle$ for the prismatic, basal and pyramidal π_1 planes (Fig. 4). For both Ti and Zr, the profile corresponding to the prismatic plane has a local minimum for a translation vector of $\langle a \rangle/2$, which corresponds to the stable prismatic fault configuration. This minimum is obtained neither by existing empirical potentials (Ti [94]) nor by the TB model used by Legrand [91] or that of Girshick et al. [94].

The excess energy profile along the $\langle c + a \rangle$ Burgers vector for the π_1 and π_2 pyramidal planes look both similar [92] with much higher energy profiles. Both profiles have a local minimum close to $\langle c + a \rangle/2$, the excess energy being nevertheless high enough (400–500 mJ/m²) to prevent from a significant dislocation core dissociation.

The hydrogen influence on dislocation mobility has been investigated in an indirect way, by placing H atoms at the stacking fault plane using different coverage ratios [50]. For both Zr and Ti, in basal and prismatic fault planes, the presence of H induces a significant fault energy decrease (see Table 15) enhanced by the H coverage. In some cases, the stacking fault energy may become negative, a result that has been associated to the existence of hydrides with high formation enthalpy [50]. Since the screw dislocation core may be seen as an ‘incipient’ prismatic fault, it is likely that H atoms should segregate to the dislocation core (in this case the driving force is purely chemical since there is no first order elastic interaction between screw dislocations and H atoms). Due to the H-induced stacking fault energy reduction the prismatic spreading will increase leading to an enhanced planar glide.

4.2. Dislocation core structure

There are two approaches to determine the dislocation core structure from ab initio calculation. The first one is based on the Peierls Nabarro model, and

Table 14
Zr and Ti excess stacking fault energies, shear elastic constants and Legrand ratio [91]

		γ_{bas} (mJ/m ²)	γ_{prism} (mJ/m ²)	C_{44} (GPa)	C_{66} (GPa)	R
Zr	Ab initio GGA	200 (237)	145 (455)	29	39	1.9
	TB [91]	340	150	42	42	2.3
	Exp.	–	–	36.3	44	Prismatic
Ti	Ab initio GGA	291	174	43	45	1.8
	TB [91]	290	110	45	43	2.5
	Exp.	–	150 [93]	46.7	35	Prismatic

In parenthesis values of the stacking fault energy without atomic relaxations.

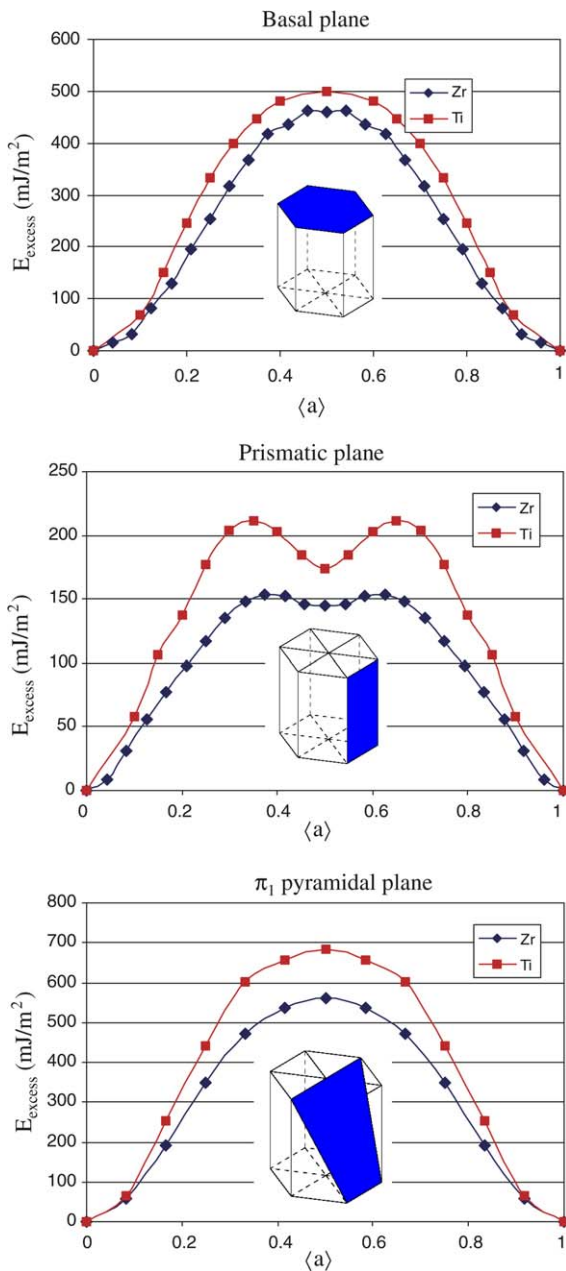


Fig. 4. Gamma-surface excess energy (in mJ/m^2) profile along $\langle a \rangle$ in the basal, prismatic and pyramidal π_1 slip planes for Zr and Ti. The relaxation of the distance between the atomic planes surrounding the fault plane (in \AA) is plotted in Zr for the basal and prismatic planes.

the core spreading is obtained solving equation sets with the generalised stacking fault energy determined by ab initio calculations. The core structure in several transition metals (e.g. Ni_3Al [95], Al and Ag [96]) and semiconductors (e.g. Si [97]) have been predicted. The second approach is the direct relaxa-

Table 15

Effect of hydrogen on basal and prismatic stacking fault energy in Zr and Ti (in mJ/m^2)

Coverage, θ	Basal plane		Prismatic plane	
	Zr	Ti	Zr	Ti
0	200	291	145	174
0.25	80	102	73	72
0.5	-60	-105	67	66
1	-14	-54	-90	-190

The coverage ratio θ is the ratio between occupied and available number of tetrahedral sites in between the atomic planes surrounding the fault plane before the fault vector is applied.

tion of the core, which is necessary for non-planar core for which the core structure is more complex. Such complex cores are found for screw dislocation in bcc and hcp metals. In these metals, the core structure of screw dislocation is a key issue related to the dislocation mobility and plasticity at low temperature [98,99].

The direct core structure of $\langle 111 \rangle$ screw dislocation in bcc transition metals have been determined for Fe [100], Mo [100–103], Ta [101–103]. The ab initio calculations predict a core structure less spread than the one obtained with empirical potentials by molecular dynamics. For Mo and Fe, Frederiksen and Jacobsen [100] have found that the screw dislocation cores are symmetric with respect to 180° rotations around an axis perpendicular to the dislocation line. In hcp metals such as Ti or Zr, the spreading of the screw dislocation core is also a key issue and has been only calculated by ab initio on small system for Zr [104].

We have determined the core structure of the $\langle a \rangle$ screw dislocation for Ti and Zr using supercell up to 61 and 127 atoms. Whatever the cell simulation size (61 or 127 atoms) [92], both Zr and Ti present similar trends: the core has a marked prismatic spreading with screw character while a secondary spreading with and edge component is observed along the basal planes (Figs. 5 and 6).

Starting from the geometrical configuration, the fully relaxed structure depicted in Figs. 5 and 6 is obtained only if the atoms are allowed to move along and perpendicularly to the dislocation line. The sole relaxation parallel to the line does not entail significant modifications with respect to the geometrical configuration. This fact illustrates the importance of the edge character atomic relaxation to obtain a correct core structure. As illustrated by Fig. 5, the strongest edge relaxation component is parallel to the c -axis.

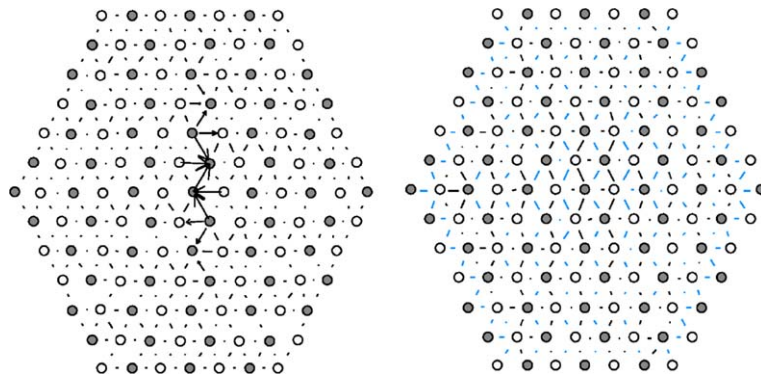


Fig. 5. Zr screw dislocation core, screw component (on the right) and edge component (on the left) of the displacement (127 atoms). The empty and filled circles allow to distinguish the initial two different atomic planes.

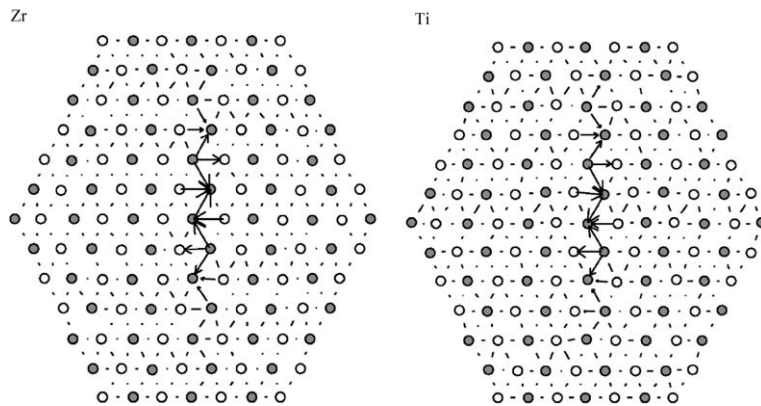


Fig. 6. Screw dislocation core of Zr and Ti (screw component of the displacement, 127 atoms).

These trends are almost independent on the cell size for cells containing between 61 and 127 atoms. The prismatic spreading, of the order of $3c$, is quite well converged even using a 61-atom supercell. The secondary basal spreading, smaller than the primary prismatic one, seems to be long-range as shown by Fig. 6 obtained using the larger cells. It is important to point out that the previously mentioned discrepancies between atomic scale potentials concerning the atomic relaxations around the prismatic fault may induce significant differences in the secondary spreading, modifying not only the core structure but also the dislocation mobility.

5. Conclusions

Ab initio calculations can provide a large set of configurations and energies at the atomic scale. These information can allow to define some elementary physical phenomenon: point defect formation

energies, defect-solute binding energies, stacking fault energies, dislocation core structure.

These ab initio have confirmed or gave insights for the following mechanisms:

The $\langle 110 \rangle$ self-interstitial in bcc Fe is the most stable configuration. The self-interstitial energy formation in hcp Zr are low and close together.

C and N are bounded to vacancy, and the formation of 2FIAs – vacancy complexes lead to very stable structure, with formation of covalent bond for C.

As a rare gas, He prefer substitutional position, and tetrahedral configuration is the most stable interstitial position with similar behaviour in Fe, Cr and Ni.

In bcc Fe, solute atom interactions with vacancy is not straight forward link to elastic interaction due to solute size effect, but chemical interactions seem to play an important role. P in bcc Fe and Nb in Zr have both a strong interaction with self-interstitial atoms which may have effects under irradiation.

A low prismatic stacking fault energy is obtained for hcp Zr and Ti compared to the basal stacking fault. In addition, the core structure of $\langle a \rangle$ screw dislocation in Zr and Ti are similar and present a prismatic spreading with some secondary spreadings in the basal plane. The results are in agreement with the experimentally known motion of screw dislocation in the prismatic plane for these metals. In addition, hydrogen tends to reduce the stacking fault energies.

The ab initio data can be used to develop a cohesive model for the upper scale within the multiscale modelling approach: (i) to fit empirical potentials for short time scale kinetic (molecular dynamics simulations); (ii) to get energetic models for medium term kinetic evolution (atomic Monte Carlo); (iii) to get binding energies and defect mobilities for long term kinetic and evolution (object or event kinetic Monte Carlo, cluster dynamics); (iv) to get segregation energies for segregation kinetic models (mean field approaches); (v) to get information on the dislocation behaviour (dislocation dynamics, through molecular dynamics).

Improved inputs from ab initio calculations should be obtained by the use of larger supercells for cluster defects or extended defects.

Another way of improvement is the amelioration of the ab initio calculation with a better treatment of the magnetism, by doing non-collinear calculations. This treatment requires larger computing resources, but may lead to more predictive values in cases such as Mn in Fe, or fcc Fe (for austenitic steels modelling), for which the magnetism is known to be complex.

The determination of the activation barriers for the defect migration is a vast subject that still needs to be explored in more details in order to improve the kinetic predictions of upper scale methods such as kinetic Monte Carlo or rate theory.

Acknowledgements

The author acknowledges C.S. Becquart and A. Legris for fruitful discussions and collaboration and for a critical reading of the manuscript.

This work has been performed within the Euratom European PERFECT project (FI6O-CT-2003-508840), the SIRENA project (SIR1-CT-2001-20137) and the ITEM network (FIR1-CT2001-20163) which has sponsored this study. This research has been done using the CRI supercomputer of the USTL supported by the Fonds Européens de Développement

Régional, as well as the CEA CCRT supercomputers in the framework of an EDF-CEA contract.

Appendix A. Calculation technical details

This appendix contains the conditions of our simulations and the equilibrium bulk properties of Fe, Zr and Ti.

The equilibrium lattice parameter for Fe used with USPP is 2.8544 Å.

The equilibrium lattice parameters of hexagonal Zr and Ti are given below.

	a (Å)	c (Å)	c/a
Zr	3.239	5.163	1.594
Zr exp	3.232	5.149	1.593
Ti	2.940	4.672	1.589
Ti exp	2.95	4.68	1.586

The different plane wave energy cut-offs used are summarised in the table below.

System	Cut-off energy (eV)
Fe with all elements except C and He	240
Fe with C	290
Fe with He	350 and 400
Zr	240
Cr–He	400
Ni–He	400

References

- [1] G.R. Odette, B.D. Wirth, D.J. Bacon, N.M. Ghoniem, *MRS Bull.* 26 (2001) 176.
- [2] N.M. Ghoniem, E.P. Busso, N. Kioussis, H. Huang, *Philos. Mag.* 83 (2003) 3475.
- [3] C.S. Becquart, *Nucl. Instrum. and Meth. Phys. B* 228 (2005) 111.
- [4] S. Jumel, C. Domain, J. Ruste, J.C. Van Duysen, C. Becquart, A. Legris, P. Pareige, A. Barbu, E. Van Walle, R. Chaouadi, M. Hou, R. Odette, R. Stoller, B.D. Wirth, *J. Testing Eval.* 30 (2002) 37.
- [5] L. Malerba, E. van Walle, C. Domain, S. Jumel, J.C. van Duysen, in: *Proceedings of ICONE-10: 10th International Conference on Nuclear Engineering*, Arlington, USA, 2002.
- [6] <http://www.fp6perfect.net>.
- [7] C. Domain, C.S. Becquart, *J. Phys. Rev. B* 69 (2004) 144112.
- [8] P. Hohenberg, W. Kohn, *Phys. Rev.* 136 (1964) 864.
- [9] W. Kohn, L. Sham, *Phys. Rev. B* 140 (1965) 1133.

- [10] R.G. Parr, W. Yang, *Density Functional Theory of Atoms and Molecules*, Oxford University Press, 1989.
- [11] M. Sifkovits, H. Smolinski, S. Hellwig, W. Weber, *J. Mag. Mag. Mater.* 204 (1999) 191.
- [12] S. Ishida, K. Kitawatase, S. Fujii, S. Asano, *J. Phys.: Condens. Mater.* 4 (1992) 765.
- [13] Y. Kong, *J. Phys.: Condens. Matter* 12 (2000) 4161.
- [14] A.V. dos Santos, M.I. da Costa, C.A. Kuhnen, *J. Mag. Mag. Mater.* 166 (1997) 223.
- [15] H.C. Herper, D. Hoffmann, P. Entel, *Phys. Rev. B* 60 (1999) 3839.
- [16] D.B. Laks, L.G. Ferreira, S. Froyen, A. Zunger, *Phys. Rev. B* 46 (1992) 12587.
- [17] C. Wolverton, V. Ozolips, A. Zunger, *Phys. Rev. B* 57 (1998) 4432.
- [18] V. Ozolips, C. Wolverton, A. Zunger, *Phys. Rev. B* 57 (1998) 6427.
- [19] C. Colinet, *Calphad* 25 (2001) 607.
- [20] S. Shang, A.J. Böttger, *Acta Mater.* 53 (2005) 255.
- [21] S. Tang, A.L. Freeman, G.B. Olson, *Phys. Rev. B* 47 (1993) 2441.
- [22] L. Zhong, R.Q. Wu, A.L. Freeman, G.B. Olson, *Phys. Rev. B* 55 (1997) 11133.
- [23] L.P. Sagert, G.B. Olson, D.E. Ellis, *Philos. Mag. B* 77 (1998) 871.
- [24] P. Rez, J.R. Alvarez, *Acta Mater.* 47 (1999) 4069.
- [25] C. Woodward, *Mater. Sci. Eng. A* 400&401 (2005) 59.
- [26] M.I. Mendeleev, S. Han, D.J. Srolovitz, G.J. Ackland, D.Y. Sun, M. Asta, *Philos. Mag.* 83 (2003) 3977.
- [27] Z. Tang, M. Hasegawa, Y. Nagai, M. Saito, Y. Kawazoe, *Phys. Rev. B* 65 (2001) 045108.
- [28] Z. Tang, M. Hasegawa, Y. Nagai, M. Saito, *Phys. Rev. B* 65 (2001) 195108.
- [29] J. Hafner, *Acta Mater.* 48 (2000) 71.
- [30] M.C. Payne, M.P. Teter, D.C. Allan, T.A. Arias, J.D. Joannopoulos, *Rev. Mod. Phys.* 64 (1992) 1045.
- [31] D. Hobbs, G. Kresse, J. Hafner, *Phys. Rev. B* 62 (2000) 11556.
- [32] M. Marsman, J. Hafner, *Phys. Rev. B* 66 (2002) 224409.
- [33] R. Hafner, D. Spisak, R. Lorenz, J. Hafner, *J. Phys. Condens. Matter* 13 (2001) L239.
- [34] D. Hobbs, J. Hafner, D. Spišák, *Phys. Rev. B* 68 (2003) 014407.
- [35] V.J. Anisimov, J. Zaanen, O. Andersen, *Phys. Rev. B* 44 (1991) 943.
- [36] J.P. Perdew, A. Zunger, *Phys. Rev. B* 23 (1981) 5048.
- [37] L. Hedin, S. Lundqvist, *Solid State Phys.* 23 (1969) 1.
- [38] S.G. Louie, in: J.R. Chelikowsky, S.G. Louie (Eds.), *Quantum Theory of Real Materials*, Kluwer, Massachusetts, 1996, p. 83.
- [39] G.H. Vineyard, *J. Phys. Chem. Solids* 3 (1957) 121.
- [40] G. Kresse, J. Hafner, *Phys. Rev. B* 47 (1993) 558; G. Kresse, J. Hafner, *Phys. Rev. B* 49 (1994) 14251.
- [41] G. Kresse, J. Furthmüller, *Phys. Rev. B* 54 (1996) 11169; G. Kresse, J. Furthmüller, *Comput. Mater. Sci.* 6 (1996) 15.
- [42] D. Vanderbilt, *Phys. Rev. B* 41 (1990) 7892.
- [43] G. Kresse, J. Hafner, *J. Phys.: Condens. Mater.* 6 (1996) 8245.
- [44] J.P. Perdew, Y. Wang, *Phys. Rev. B* 45 (1991) 13244.
- [45] P.E. Blöchl, *Phys. Rev. B* 50 (1994) 17953.
- [46] G. Kresse, D. Joubert, *Phys. Rev. B* 59 (1999) 1758.
- [47] H.J. Monkhorst, J.D. Pack, *Phys. Rev. B* 13 (1976) 5188, In the original Monkhorst and Pack scheme, the k point mesh is always symmetric around the Γ point, whereas very often in our calculations we adopted grids centred at the Γ point.
- [48] C. Domain, C.S. Becquart, *Phys. Rev. B* 65 (2002) 024103.
- [49] S. Rao, C. Hernandez, J.P. Simmons, T.A. Parthasarathy, C. Woodward, *Philos. Mag. A* 77 (1998) 231.
- [50] C. Domain, A. Legris, R. Besson, *Acta Mater.* 52 (2004) 1495.
- [51] V. Vitek, R.C. Perrin, D.K. Bowen, *Philos. Mag.* 21 (1970) 1049.
- [52] P. Söderlind, L.H. Yang, J.A. Moriarty, J.M. Wills, *Phys. Rev. B* 61 (2000) 2579.
- [53] B. Meyer, M. Fähnle, *Phys. Rev. B* 56 (1997) 13595.
- [54] A. Satta, F. Willaime, S. de Gironcoli, *Phys. Rev. B* 60 (1999) 7001.
- [55] A. Satta, F. Willaime, S. de Gironcoli, *Phys. Rev. B* 57 (1998) 11184.
- [56] C.C. Fu, F. Willaime, P. Ordejon, *Phys. Rev. Lett.* 92 (2004) 175503.
- [57] C. Domain, A. Legris, *Philos. Mag.* 85 (2005) 569.
- [58] F. Willaime, *J. Nucl. Mater.* 323 (2003) 205.
- [59] S.W. Han, L.A. Zepeda-Ruiz, G.J. Ackland, R. Car, D.J. Srolovitz, *Phys. Rev. B* 66 (2002) 220101.
- [60] R.A. Johnson, *Phys. Rev.* 134 (1964) A1329.
- [61] G. Simonelli, R. Pasianot, E.J. Savino, *Phys. Rev. B* 50 (1994) 727.
- [62] G.J. Ackland, D.J. Bacon, A.F. Calder, T. Harry, *Philos. Mag. A* 75 (1997) 713.
- [63] G.J. Ackland, *Philos. Mag. A* 66 (1992) 66.
- [64] R.C. Pasianot, A.M. Monti, *J. Nucl. Mater.* 264 (1999) 198.
- [65] C.S. Becquart, C. Domain, *Nucl. Instrum. and Meth. Phys. B* 202 (2003) 44.
- [66] F. Willaime, C.C. Fu, M.C. Marinica, J. Dalla Torre, *Nucl. Instrum. and Meth. Phys. B* 228 (2005) 92.
- [67] C.C. Fu, J. Dalla Torre, F. Willaime, J.L. Bocquet, A. Barbu, *Nature Mater.* 4 (2005) 68.
- [68] C. Domain, C.S. Becquart, L. Malerba, *J. Nucl. Mater.* 335 (2004) 121.
- [69] P. Rochegude, J. Foct, *Phys. Stat. Sol. (a)* 98 (1986) 51.
- [70] R.A. Johnson, G.J. Dienes, A.C. Damask, *Acta Met.* 12 (1964) 1215.
- [71] V. Rosato, *Acta Met.* 37 (1989) 2759.
- [72] M. Weller, *J. Phys.* 46 (1985) C10.
- [73] Y. Fukai, *The Metal Hydrogen System*, Springer-Verlag, 1992.
- [74] G.V. Kidson, Numerical data and functional relationships in science and technology, in: H. Mehrer (Ed.), *Landolt-Börnstein, New Series III*, 26, Springer-Verlag, 1990, p. 528, Chapter 9.
- [75] C. Domain, Thesis, Université de Lille and EDF, 2002.
- [76] D.E. Jiang, E. Carter, *Phys. Rev. B* 67 (2003) 214103.
- [77] C. Domain, R. Besson, A. Legris, *Acta Mater.* 50 (2002) 3513.
- [78] R.A. Arndt, A.C. Damask, *Acta Met.* 12 (1964) 341; F.E. Fujita, A.C. Damask, *Acta Met.* 12 (1964) 331.
- [79] S. Takaki, J. Fuss, H. Kugler, U. Dedek, H. Schults, *Radiat. Eff.* 79 (1983) 87.
- [80] A. Vehanen, P. Hautojärvi, J. Johansson, J. Yli-Kaupilla, P. Moser, *Phys. Rev. B* 25 (1982) 762.
- [81] P. Hautojärvi, J. Johansson, A. Vehanen, J. Yli-Kaupilla, *Phys. Rev. Lett.* 44 (1980) 1326.

- [82] T. Seletskaja, Y. Osetsky, R.E. Stoller, G.M. Stocks, *Phys. Rev. Lett.* 94 (2005) 046403.
- [83] H. Ullmaier, *Radiat. Eff.* 78 (1983) 1.
- [84] D.J. Reed, *Radiat. Eff.* 31 (1977) 129.
- [85] L. Ventelon, B.D. Wirth, C. Domain, *J. Nucl. Mater.* 351 (2006) 119.
- [86] E. Vincent, C.S. Becquart, C. Domain, *Nucl. Instrum. and Meth. Phys. B* 228 (2005) 137.
- [87] E. Vincent, C.S. Becquart, C. Domain, *J. Nucl. Mater.* 351 (2006) 88.
- [88] C. Domain, C.S. Becquart, *Phys. Rev. B* 71 (2005) 214109.
- [89] A. Möslang, E. Albert, E. Rcknagel, A. Weindiger, *Hyperfine Interact.* 15&16 (1983) 409.
- [90] G.J. Ackland, M.I. Mendeleev, D.J. Srolovitz, S. Han, A.V. Barashev, *J. Phys.: Condens. Matter.* 16 (2004) S2629.
- [91] B. Legrand, Thesis, Orsay University, 1884.
- [92] C. Domain, A. Legris, Proceedings IUTAM, Osaka, 2004.
- [93] A. De Crecy, A. Bourret, S. Naka, A. Lasalmonie, *Phil Mag A* 47 (1983) 245.
- [94] A. Girshick, D.G. Pettifor, V. Vitek, *Philos. Mag. A* 77 (1998) 999.
- [95] G. Schoeck, *Philos. Mag. Lett.* 79 (1999) 849.
- [96] G. Lu, V.V. Bulatov, N. Kioussis, *Philos. Mag.* 83 (2003) 3539.
- [97] B. Joos, Q. Ren, M.S. Duesbery, *Phys. Rev. B* 50 (1994) 5890.
- [98] L.P. Kubin, *Reviews on the deformation behavior of materials 1* (1976) 243.
- [99] J.W. Christian, *Met. Trans. A.* 14A (1983) 1237.
- [100] S.L. Frederiksen, K.W. Jacobsen, *Philos. Mag. A* 83 (2003) 365.
- [101] S. Ismail-Beigi, T.A. Arias, *Phys. Rev. Lett.* 84 (2000) 1499.
- [102] C. Woodward, S.I. Rao, *Philos. Mag. A* 81 (2001) 1305.
- [103] C. Woodward, S.I. Rao, *Phys. Rev. Lett.* 88 (2002) 216402.
- [104] F. Ferrer, PhD Thesis, Ecole Polytechnique, 2000.
- [105] J.D. Fast, M.B. Verrijp, *J. Iron Steel Inst.* 176 (1954) 24.
- [106] A.D. Le Claire, Numerical data and functional relationships in science and technology, in: H. Mehrer (Ed.), *Landolt-Börnstein, New Series, Group III, 26*, Springer-Verlag, 1990, p. 480, Chapter 8.
- [107] C.S. Zhang, B. Li, P.R. Norton, *J. Alloys Compd.* 231 (1995) 354.
- [108] G. Brauer, K. Popp, *Phys. Stat. Sol.* 102 (1987) 79.